

Effects of encapsulation damping on the excitation threshold for subharmonic generation from contrast microbubbles

Amit Katiyar

Department of Mechanical Engineering, University of Delaware, 130 Academy Street, Newark, Delaware 19716

Kausik Sarkar^{a)}

Department of Mechanical and Aerospace Engineering, George Washington University, 802 22nd Street NW, Washington, DC 20052

(Received 4 April 2012; revised 16 September 2012; accepted 18 September 2012)

A recent study [Katiyar and Sarkar (2011). *J. Acoust. Soc. Am.* **130**, 3137–3147] showed that in contrast to the analytical result for free bubbles, the minimum threshold for subharmonic generation for contrast microbubbles does not necessarily occur at twice the resonance frequency. Here increased damping—either due to the small radius or the encapsulation—is shown to shift the minimum threshold away from twice the resonance frequency. Free bubbles as well as four models of the contrast agent encapsulation are investigated varying the surface dilatational viscosity. Encapsulation properties are determined using measured attenuation data for a commercial contrast agent. For sufficiently small damping, models predict two minima for the threshold curve—one at twice the resonance frequency being lower than the other at resonance frequency—in accord with the classical analytical result. However, increased damping damps the bubble response more at twice the resonance than at resonance, leading to a flattening of the threshold curve and a gradual shift of the absolute minimum from twice the resonance frequency toward the resonance frequency. The deviation from the classical result stems from the fact that the perturbation analysis employed to obtain it assumes small damping, not always applicable for contrast microbubbles.

© 2012 Acoustical Society of America. [http://dx.doi.org/10.1121/1.4757099]

PACS number(s): 43.80.Qf, 43.35.Ei, 43.80.Ev, 43.20.Fn [CCC]

Pages: 3576–3585

I. INTRODUCTION

Micron-size encapsulated bubbles (radius $< 10 \mu\text{m}$) are used in diagnostic ultrasound imaging as contrast enhancing agents (de Jong, 1996; Ferrara *et al.*, 2007; Goldberg *et al.*, 2001; Tang *et al.*, 2011). They generate subharmonic signals that are utilized for subharmonic imaging—imaging at frequencies half that of the excitation (Forsberg *et al.*, 2000; Shankar *et al.*, 1998; Shankar *et al.*, 1999). Variation of the subharmonic response with ambient pressure is also being investigated for developing a noninvasive organ-level blood pressure monitoring technique (Adam *et al.*, 2005; Andersen and Jensen, 2010; Dave *et al.*, 2011; Forsberg *et al.*, 2005; Frinking *et al.*, 2010; Katiyar *et al.*, 2011; Leodore *et al.*, 2007; Shi *et al.*, 1999). Therefore, accurate prediction of the subharmonic response from contrast microbubbles is a topic of great interest (Eller and Flynn, 1968; Faez *et al.*, 2011; Katiyar and Sarkar, 2011; Kimmel *et al.*, 2007; Paul *et al.*, 2010; Prosperetti, 1976, 1977; Sijl *et al.*, 2010). Bubbles generate subharmonic response only when excited above a threshold pressure. It is widely believed that the minimum threshold for subharmonic generation occurs at twice the resonance frequency ($2f_0$)—a result obtained using a perturbative analysis on free bubble dynamics (Eller and Flynn,

1968; Prosperetti, 1977). In a recent paper, hereafter referred to as KS1 (Katiyar and Sarkar, 2011), we investigated a number of existing models for encapsulated contrast microbubbles to show that the minimum threshold for subharmonic generation does not occur at $2f_0$; it occurs over a range of frequencies from f_0 to $2f_0$. Specifically, for some models, the minimum threshold occurs at f_0 . Here, we further investigate this phenomenon to understand the apparent contradiction. Specifically, we examine the role of enhanced damping due to the encapsulation of a contrast microbubble on subharmonic threshold.

In KS1, we investigated the frequency-dependent subharmonic threshold according to six different models of contrast microbubbles—(1) Newtonian model, (2) de Jong model, (3) Church–Hoff model, (4) constant surface elasticity model, (5) Marmottant model, and (6) strain-softening exponential surface elasticity model (Katiyar and Sarkar, 2011). The Newtonian interfacial rheological model is the first interfacial rheological model proposed in the contrast agent literature (Chatterjee and Sarkar, 2003). Interfacial rheological models treat an encapsulation as a zero-thickness complex interface—an appropriate approach keeping in view the wide disparity of length-scales between the encapsulation (approximately nanometer thickness) and the overall microbubble (approximately micrometer radius). In this approach, the encapsulation stresses are determined by the intrinsic interfacial rheology (as opposed to the bulk rheology of the material of the encapsulation).

^{a)} Author to whom correspondence should be addressed. Also at: Department of Mechanical Engineering, University of Delaware, 130 Academy Street, Newark, DE 19716. Electronic mail: sarkar@gwu.edu

In recent years, other interfacial rheological models have been proposed to incorporate various aspects of the encapsulation dynamics. In KS1, all six models, including those due to Church–Hoff (Church, 1995; Hoff *et al.*, 2000) and de Jong (de Jong *et al.*, 1994), which were not originally interfacial models, were presented in an effective interfacial rheology form. The bubble dynamics was described by a generalized Rayleigh–Plesset (RP) equation, with an effective surface tension $\gamma(R)$ and an effective dilatational surface viscosity $\kappa^s(R)$ (R is the instantaneous bubble radius). Each model was numerically investigated to find the minimum subharmonic threshold for Sonazoid (GE Health Care, Oslo, Norway) contrast microbubble. As mentioned previously, the minimum threshold for many models was found to occur not at $2f_0$, but over a range from f_0 to $2f_0$. We found that the form of $\gamma(R)$ plays a crucial role. The constant surface elasticity model (Sarkar *et al.*, 2005) and the de Jong model predict unusually high values of subharmonic threshold with a minimum at $2f_0$. However, the Marmottant model (Marmottant *et al.*, 2005), which also assumes a constant surface elasticity but only between two radius limits—an upper limit where the encapsulation ruptures and a lower limit where the encapsulation buckles—predicts a valley of minima from f_0 to $2f_0$. The strain-softening exponential surface elasticity model proposed recently by Paul *et al.* (2010), as well as the Church–Hoff model, have natural upper limits on surface tension. Both models show behaviors similar to the Marmottant model. We concluded that the absence of an upper limit on surface tension results in a very high subharmonic threshold near resonance, and correspondingly the minimum threshold is obtained at $2f_0$. However, introducing a maximum limit on surface tension—due to encapsulation rupture at large extension—lowers the threshold at resonance, and leads to comparable thresholds over the range.

In KS1, the interfacial dilatational viscosity κ^s (assumed constant for each model except for the Church–Hoff model, where it varies naturally with radius) represented an additional damping contribution due to the encapsulation. It adds to the other three damping elements present in the case of a free bubble arising from liquid viscosity, thermal effects and acoustic radiation. The thermal damping is often negligible for contrast microbubbles. Note that all three other damping terms [see the upcoming Eq. (3)] increase with decreasing bubble radius, thereby resulting in a large damping for contrast agents due to their small (micrometer) size. For the bubble considered ($R_0 = 3 \mu\text{m}$) in KS1 (although the average radius of a Sonazoid bubble is $1.6 \mu\text{m}$, the representative radius of the bubbles responsible for subharmonic generation was shown in KS1 to be $3 \mu\text{m}$), the different nondimensional damping terms were $\delta_{\text{liquid}} = 0.04$ for the liquid, $\delta_{\text{radiation}} = 0.006$ for radiation and $\delta_{\text{encapsulation}} = 0.13$ for the encapsulation. The damping due to the encapsulation is an order of magnitude higher than the other two present in a free bubble. We note that the prediction of minimum threshold being at twice the linear resonance frequency was obtained using a perturbation analysis for a lightly damped system. The result represents the physics that a system would naturally generate transient response at its resonance frequency, which is

amenable to an easy amplification by nonlinear energy transfer. For bubble dynamics, the analytical result (Eller and Flynn, 1968; Prosperetti, 1977) was obtained by a perturbative method that specifically assumed small bubble oscillations excited at frequencies near $2f_0$. However, in actual experiments both *in vitro* and *in vivo*, as well as in clinical setting, ultrasound pulses are applied containing a wide band of frequencies. Also, as the excitation frequency approaches resonance, the oscillations are not small and perturbative result might lose its validity. Prosperetti (1977) reported a strong sensitivity of subharmonic threshold on damping near twice the resonance frequency. Therefore, for an encapsulated contrast microbubble with its large damping, one has to rely on numerical simulation for accurate prediction of its dynamics. Finally, Faez *et al.* (2012) very recently have found that increased viscosity in a chicken embryo led to a lower subharmonic generation threshold for subharmonic generation for a lipid coated microbubble at f_0 than at $2f_0$ —at 300–400 kPa excitation, subharmonic response was recorded at the resonance frequency, but not at twice its value. Also note that in our previous experimental investigation of a Sonazoid suspension (Paul *et al.*, 2010; Sarkar *et al.*, 2005), although the minimum threshold for subharmonic generation was not investigated, the subharmonic threshold was seen to steadily decrease in the range of frequencies considered from 2 MHz to 6 MHz indicating the minimum threshold to be away from twice the resonance frequency.

In this paper, we numerically investigate the (1) free bubble model, (2) Newtonian model, (3) Church–Hoff model, (4) Marmottant model, and (5) strain-softening exponential surface elasticity model. The apparent contradiction with the classical subharmonic threshold result seen in KS1, gives rise to the following consideration. In KS1, we used f_0 of the undamped system corresponding to the bubble dynamics. However, the frequency of maximum response of a damped mass-spring system typically decreases with increasing amount of damping δ . One possible explanation of the observation in KS1 of minimum threshold at frequencies lower than $2f_0$ in contrast to classical result can be sought in this decrease in natural frequency. We first investigate this hypothesis in the following. In the next section, we briefly describe these models and discuss different damping mechanisms. In Sec. III, we show how variation in initial bubble radius and interfacial dilatational viscosity of an encapsulation affect the total damping, as well as the subharmonic threshold. Finally, Sec. IV summarizes the results. As in KS1, bubble breakup is not considered, although at larger excitation, bubbles undergo breakup by distinct mechanisms (Chatterjee *et al.*, 2005a).

II. MATHEMATICAL FORMULATION AND NUMERICAL SOLUTION

The models—free, as well as the five encapsulated contrast microbubbles—have been described in detail in KS1. Here, we briefly repeat the description by stating the equations for the sake of completeness. A compressible form of the RP equation is used to describe the time evolution of the radius R of a contrast microbubble,

$$\rho \left(R\ddot{R} + \frac{3}{2}\dot{R}^2 \right) = P_{G_0} \left(\frac{R_0}{R} \right)^{3k} \left(1 - \frac{3k\dot{R}}{c} \right) - \frac{2}{R}\gamma(R) - \frac{4\dot{R}}{R^2}\kappa^s - 4\mu\frac{\dot{R}}{R} - p_0 + p_A, \quad (1)$$

where R_0 is the initial bubble radius, \dot{R} and \ddot{R} are the first- and the second-order time derivatives of the bubble radius R , P_{G_0} is the initial gas pressure inside the bubble, k is the polytropic exponent, ρ is the liquid density, μ is the liquid viscosity, γ is the gas–liquid surface tension, p_0 is the ambient pressure, p_A is the excitation pressure with amplitude P_A , and c is the sound velocity in liquid. Gas diffusion from the bubble is neglected. Surface tension $\gamma(R)$ and the interfacial dilatational viscosity κ^s characterize the interfacial rheology of the bubble encapsulation.

A. Free bubble and Newtonian (Chatterjee and Sarkar, 2003) model

For the Newtonian model,

$$\gamma(R) = \gamma, \quad \kappa^s(R) = \kappa^s, \quad (2)$$

both are constant. In the case of a free bubble $\kappa^s = 0$ and $\gamma(R) = \gamma_w$, surface tension at the gas–water interface. From the linearized form of Eq. (1), one obtains the nondimensional damping constant (δ) and the linear resonance frequency ($f_0 = \omega_0 / 2\pi$),

$$\begin{aligned} \delta &= \delta_{\text{liquid}} + \delta_{\text{encapsulation}} + \delta_{\text{radiation}} \\ &= \frac{4\mu}{\rho\omega_0 R_0^2} + \frac{4\kappa^s}{\rho\omega_0 R_0^3} + \frac{3kp_0}{\rho\omega_0 R_0 c}, \end{aligned} \quad (3)$$

$$\gamma(R) = \begin{cases} 0 & \text{for } R \leq R_{\text{buckling}} \\ \chi \left(\frac{R^2}{R_{\text{buckling}}^2} - 1 \right) & \text{for } R_{\text{buckling}} \leq R \leq R_{\text{rupture}} \\ \gamma_w & \text{for } R \geq R_{\text{rupture}}. \end{cases}, \quad \kappa^s(R) = \kappa^s \quad (7)$$

Here χ is the elastic compression modulus, $R_{\text{buckling}} = R_0[1 + \gamma(R_0)/\chi]^{-1/2}$ is the buckling radius and $R_{\text{rupture}} = R_{\text{buckling}}[1 + \gamma_w/\chi]^{1/2}$ is the rupture radius. The damping remains the same as in Eq. (3). The resonance frequency for the Marmottant model (Marmottant *et al.*, 2005; van der Meer *et al.*, 2007) is

$$f_0 = \frac{1}{2\pi R_0} \sqrt{\frac{1}{\rho} \left(3kp_0 - \frac{2\gamma(R_0)}{R_0} (3k-1) + \frac{4\chi}{R_0} \right)}. \quad (8)$$

Note that as discussed in KS1, if the bubble initially is in a buckled state, the surface tension there is not differentiable and therefore, there is no analytically defined resonance frequency, and one has to numerically determine the frequency of maximum response.

$$f_0 = \frac{1}{2\pi R_0} \sqrt{\frac{1}{\rho} \left(3kp_0 + \frac{2\gamma}{R_0} (3k-1) \right)}. \quad (4)$$

B. Church–Hoff model (Church, 1995; Hoff *et al.*, 2000)

The Church–Hoff model is as follows:

$$\gamma(R) = 6G_s d_{\text{sh}_0} \frac{R_0^2}{R^2} \left(1 - \frac{R_0}{R} \right), \quad \kappa^s(R) = 3\mu_s d_{\text{sh}_0} \frac{R_0^2}{R^2} \quad (5)$$

Note that it models the encapsulation as a layer of finite thickness d_{sh_0} containing a viscoelastic material with shear modulus G_s and shear viscosity μ_s . It has been put in an interfacial rheological form. The nondimensional damping constant remains the same as in Eq. (3), except of course $\kappa^s \rightarrow \kappa^s \sim 3\mu_s d_{\text{sh}_0}$ for small amplitude oscillation—decreasing with increasing radius (shear thinning). The resonance frequency is

$$f_0 = \frac{1}{2\pi R_0} \sqrt{\frac{1}{\rho} \left(3kp_0 + 12G_s \frac{d_{\text{sh}_0}}{R_0} \right)}. \quad (6)$$

C. Marmottant model (Marmottant *et al.*, 2005)

The Marmottant model is as follows:

D. Exponential elasticity model (EEM)

(Paul *et al.*, 2010):

The exponential elasticity model is as follows:

$$\gamma(R) = \gamma_0 + E^s \beta, \quad E^s = E_0^s \beta \exp(-\alpha^s \beta), \quad \kappa^s(R) = \kappa^s. \quad (9)$$

Here $\beta = (R^2 - R_E^2) / R_E^2$ is the change in area fraction and R_E is the equilibrium radius with zero elastic stress,

$$R_E = R_0 \left[1 + \left(\frac{1 - \sqrt{1 + 4\gamma_0 \alpha^s / E_0^s}}{2\alpha} \right) \right]^{-1/2}, \quad (10)$$

γ_0 is the constant surface tension in the undeformed state, and E_0^s and α^s are model constants. As before, damping remains the same as in Eq. (3). The linear resonance frequency

$$f_0 = \frac{1}{2\pi R_0} \sqrt{\frac{1}{\rho} \left(3kp_0 + \frac{2E_0^s}{R_0} \left(\frac{\sqrt{1 + 4\gamma_0\alpha^s/E_0^s}}{\alpha^s} \right) (1 + 2\alpha^s - \sqrt{1 + 4\gamma_0\alpha^s/E_0^s}) \right)}. \quad (11)$$

We have previously reported the procedure to determine the values of the material parameters for a contrast agent according to a model. Experimentally measured attenuation data for that contrast agent is used for the procedure (Chatterjee *et al.*, 2005b; Paul *et al.*, 2010). The parameter values for Sonazoid bubbles are given in Table I. Please note that KS1 reported erroneously $\kappa^s = 1 \times 10^{-8}$ N s/m. It should be 1.2×10^{-8} N s/m as here. In the following, we use this set as a reference and change them to study their effects.

The scattered pressure $P_s(t)$ due to a contrast microbubble is (Paul *et al.*, 2010)

$$P_s(r, t) = \rho \frac{R}{r} (2\dot{R}^2 + R\ddot{R}). \quad (12)$$

The bubble dynamics Eq. (1) is solved using a stiff solver (ODE15S) in MATLAB[®] (The MathWorks Inc., Natick, MA) with initial conditions $R = R_0$ and $\dot{R} = 0$, and parameter values $\rho = 1000$ kg/m³, $\mu = 0.001$ kg/m s, and $c = 1485$ m/s. We obtain the fast Fourier transform of the post-transient radius–time curve. For fundamental and subharmonic responses, we use the peak values corresponding to those frequencies. The excitation frequency is normalized by the model-specific linear resonance frequency mentioned previously. With increasing excitation pressure, the subharmonic component appears; it grows quickly followed by gradual saturation and eventual disappearance. The excitation pressure just above where a distinct subharmonic peak appears and on further increase in excitation pressure shows characteristics of subharmonic response is selected as the subharmonic threshold.

TABLE I. Characteristic properties of Sonazoid microbubble according to various encapsulation models.

Encapsulation model	Contrast agent (gas/encapsulation)	Parameters
Newtonian model (Chatterjee and Sarkar, 2003)	Sonazoid (C ₄ F ₁₀ /lipid)	$\gamma = 0.6$ N/m, $\kappa^s = 1.2 \times 10^{-8}$ N s/m, and $k = 1.07$
Church–Hoff model (Hoff <i>et al.</i> , 2000)	Sonazoid (C ₄ F ₁₀ /lipid)	$G_s = 52$ MPa, $\mu_s = 0.99$ N s/m ² , $d_{sh0} = 4$ nm, and $k = 1.07$
Marmottant model (Marmottant <i>et al.</i> , 2005)	Sonazoid (C ₄ F ₁₀ /lipid)	$\gamma(R_0) = 0.02$ N/m, $\chi = 0.53$ N/m, $\kappa^s = 1.2 \times 10^{-8}$ N s/m, and $k = 1.07$
Viscoelastic exponential elasticity model (EEM) (Paul <i>et al.</i> , 2010)	Sonazoid (C ₄ F ₁₀ /lipid)	$\gamma_0 = 0.019$ N/m, $E_0^s = 0.55$ N/m, $\alpha = 1.5$, $\kappa^s = 1.2 \times 10^{-8}$ N s/m, and $k = 1.07$

III. RESULTS AND DISCUSSION

A. Damped resonance frequency: Can it explain the shift in threshold minimum?

In KS1, we found that minimum threshold for subharmonic generation occurs over a range of frequencies from f_0 and $2f_0$ in contrast to the classical perturbative result that predicted it to occur at $2f_0$. From introductory physics texts, it is well known that the infinite response at resonance of an undamped linear mass-spring system becomes bounded when damping is introduced. At the same time, the maximum response decreases and occurs at progressively lower frequencies—damped resonance frequency f_r^R —with increasing damping:

$$f_r^R = f_0 \sqrt{\left(1 - \frac{\delta^2}{2}\right)}. \quad (13)$$

Therefore, it is natural to assume that the reduced natural frequency (and thereby a lower value of twice the resonance frequency) might explain the numerically simulated lower frequencies for minimum subharmonic threshold in KS1. However the above-presented argument holds for the oscillator’s primary variable—here the radius-time response of a bubble. However, we are not investigating the subharmonic component of the radius-time response, but that of the scattered pressure. The scattered pressure is related to the radius by Eq. (12). Introducing $R(t) = R_0 + \varepsilon \exp(i2\pi ft)$, we note that

$$P_s(r, t) = \frac{\rho}{r} \left\{ -R_0^2 (2\pi f)^2 \varepsilon + O(\varepsilon^2) \right\}. \quad (14)$$

The maximum radius response ($\varepsilon(f)$) from the linearized dynamics is predicted to occur at f_r^R , where $d\varepsilon/df = 0$. However, the corresponding maximum pressure occurs at a frequency $f_r^{P_s}$ where $d(\varepsilon f^2)/df = 0$ obtaining

$$f_r^{P_s} = \frac{f_0}{\sqrt{\left(1 - \frac{\delta^2}{2}\right)}}. \quad (15)$$

Clearly, the damped resonance frequency for the pressure $f_r^{P_s}$ is greater than f_0 . The numerical simulation also shows (not shown here for brevity) that the frequency where the fundamental component of the pressure achieves its maximum is higher than f_0 . The damped resonance frequency cannot explain the downshift of the frequency of minimum threshold for subharmonic generation from $2f_0$.

B. Subharmonic threshold for a free bubble

In KS1, we saw that the threshold for subharmonic generation for a free bubble follows the classical theory; it

occurs at $2f_0$ for the values of the parameters chosen there and radius $1\ \mu\text{m} \leq R_0 \leq 5\ \mu\text{m}$. In Fig. 1, we show that the damping constant δ increases sharply when the radius is decreased below $1\ \mu\text{m}$. In the inset, we notice that the minimum subharmonic threshold at $2f_0$ for $R_0 = 0.5\ \mu\text{m}$ ($\delta = 0.265$) shifts to f_0 for $R_0 = 0.2\ \mu\text{m}$ ($\delta = 0.462$). For the intermediate radius $R_0 = 0.3\ \mu\text{m}$ ($\delta = 0.364$), the thresholds at f_0 and $2f_0$ do not differ much. The increased damping at these submicron radii damps the nonlinear oscillations at $2f_0$ leading to this shift. We further refine our conclusion in KS1, in that even for a free bubble the threshold can deviate from classical result, when the damping is significant, e.g., in extremely small bubbles.

To understand the governing mechanism and the role of damping in subharmonic generation, we plot the maximum radius (after steady state oscillation sets in) as a function of frequency in Fig. 2. Specifically, we interrogate and compare radius responses at f_0 and at $2f_0$. Note that such curves were simulated by Lauterborn (1976), where the radial response was related to the harmonic, subharmonic, and ultraharmonic responses of various orders. As was noted there, the response near f_0 relates to the main resonance (1/1), and the one near $2f_0$ relates to [1/2] subharmonic response. In Fig. 2(a), we investigate it varying R_0 at an excitation of 100 kPa. From Fig. 1, this excitation is below the threshold for subharmonic generation for bubble with $R_0 \leq 0.5\ \mu\text{m}$. In KS1, we showed that at 100 kPa, one gets a subharmonic response only near $2f_0$ that is also only for larger bubbles; there is subharmonic at $R_0 \geq 2\ \mu\text{m}$ ($\delta \leq 0.1$), but not at $R_0 = 1.6\ \mu\text{m}$. At 100 kPa, Fig. 2(a) shows distinct peaks near f_0 for all bubbles and near $2f_0$ for bubbles with $R_0 \geq 2\ \mu\text{m}$. The peak response at f_0 is larger than that at $2f_0$ for all the radii considered ($1\ \mu\text{m} \leq R_0 \leq 5\ \mu\text{m}$). The subharmonic response for $R_0 \geq 2\ \mu\text{m}$ shown at KS1 correlates with the existence of a peak at $2f_0$; the peak disappears for $R_0 \leq 1.6\ \mu\text{m}$ in conformity with the absence of a subharmonic response in the spectrum. We conclude that subharmonic is generated by large oscillations at $2f_0$ for the larger bubbles; for smaller

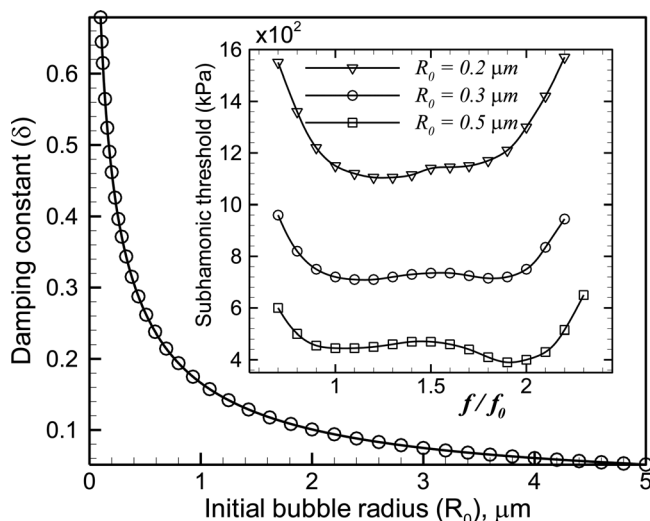


FIG. 1. Variation of the total damping constant with initial bubble radius for free bubbles. (Inset) Variation of subharmonic threshold of submicron size free bubbles with normalized excitation frequency.

bubbles, these oscillations are damped and subharmonic signal is lost. In Figs. 2(b)–2(d), we investigate three submicron radii to examine how increased damping at these smaller radii affects the radial response. We note that the peaks are progressively damped with decreasing radius. For $R_0 = 0.5\ \mu\text{m}$ [Fig. 2(b)], there is no distinct peak near f_0 , but one near $2f_0$. The peak near $2f_0$ makes it easier to generate subharmonic signal near $2f_0$. In Figs. 2(c) and 2(d), for $R_0 = 0.3\ \mu\text{m}$ and $R_0 = 0.2\ \mu\text{m}$ peaks at f_0 and $2f_0$ are diminished, and they merge into a flat rise over a broad frequency range. This small rise in the curves coincides with the appearance of a subharmonic signal. For instance, for $R_0 = 0.3\ \mu\text{m}$ and $R_0 = 0.2\ \mu\text{m}$, there is no rise in the curves at $P_A = 700\ \text{kPa}$ and $P_A = 1.15\ \text{MPa}$, respectively; for these cases there is no subharmonic response at these pressures (Fig. 1).

C. Subharmonic threshold for encapsulated microbubble

1. Newtonian model

The Newtonian model (Chatterjee and Sarkar, 2003) differs from a free bubble due to the existence of a dilatational viscosity $\kappa^s = 1.2 \times 10^{-8}\ \text{Ns/m}$ and a larger value of surface tension $\gamma = 0.6\ \text{N/m}$. Their behaviors are qualitatively similar (Fig. 3). In Fig. 3, at fixed $\kappa^s = 1.2 \times 10^{-8}\ \text{Ns/m}$, we plot a subharmonic threshold for $1.6\ \mu\text{m} \leq R_0 \leq 5\ \mu\text{m}$. For bubbles of radius $2.5\ \mu\text{m}$ and higher, the global minimum of the subharmonic threshold is obtained near $2f_0$. However, for a $2\ \mu\text{m}$ radius bubble ($\delta = 0.382$), the thresholds are comparable in the frequency range ($1 \leq f/f_0 \leq 2$). And for an even smaller bubble of $R_0 = 1.6\ \mu\text{m}$ the minimum threshold appears near f_0 . For smaller bubbles the damping due to surface dilatational viscosity significantly increases the total damping, in turn resulting in lower subharmonic thresholds near f_0 . To further highlight the role of increased damping in the shift of minimum threshold from $2f_0$ to f_0 , we varied the dilatational surface viscosity (κ^s) for a microbubble of radius $1.6\ \mu\text{m}$ and plotted the frequency-dependent subharmonic threshold in Fig. 4. Note that as κ^s decreases significantly from the predicted value of $1.2 \times 10^{-8}\ \text{Ns/m}$, the global minimum in subharmonic threshold again appears near $2f_0$ in accord with classical perturbative result.

Figure 5 shows the three damping components—due to liquid viscosity, acoustic radiation, and the encapsulation—as a function of initial radius R_0 . For a low value of dilatational viscosity $\kappa^s = 2 \times 10^{-9}\ \text{Ns/m}$, all three damping mechanisms are comparable. However, as κ^s increases, damping due to the encapsulation rises significantly for smaller radii values (e.g., for $R_0 = 1.6\ \mu\text{m}$ shown by the dashed vertical line). This increased damping leads to thresholds for subharmonic generation with no distinct minimum near $2f_0$, but a valley of similar values over the range $1 \leq f/f_0 \leq 2$ as shown in Fig. 4. Note that the plot holds also for Marmottant and exponential elasticity models, both having constant κ^s .

Note that for $R_0 = 1.6\ \mu\text{m}$, the number average radius of Sonazoid, this model predicts a very high threshold excitation for subharmonic generation of $1.4\ \text{MPa}$ (Fig. 3) in contrast to the experimentally observed value of $\sim 200\text{--}350\ \text{kPa}$

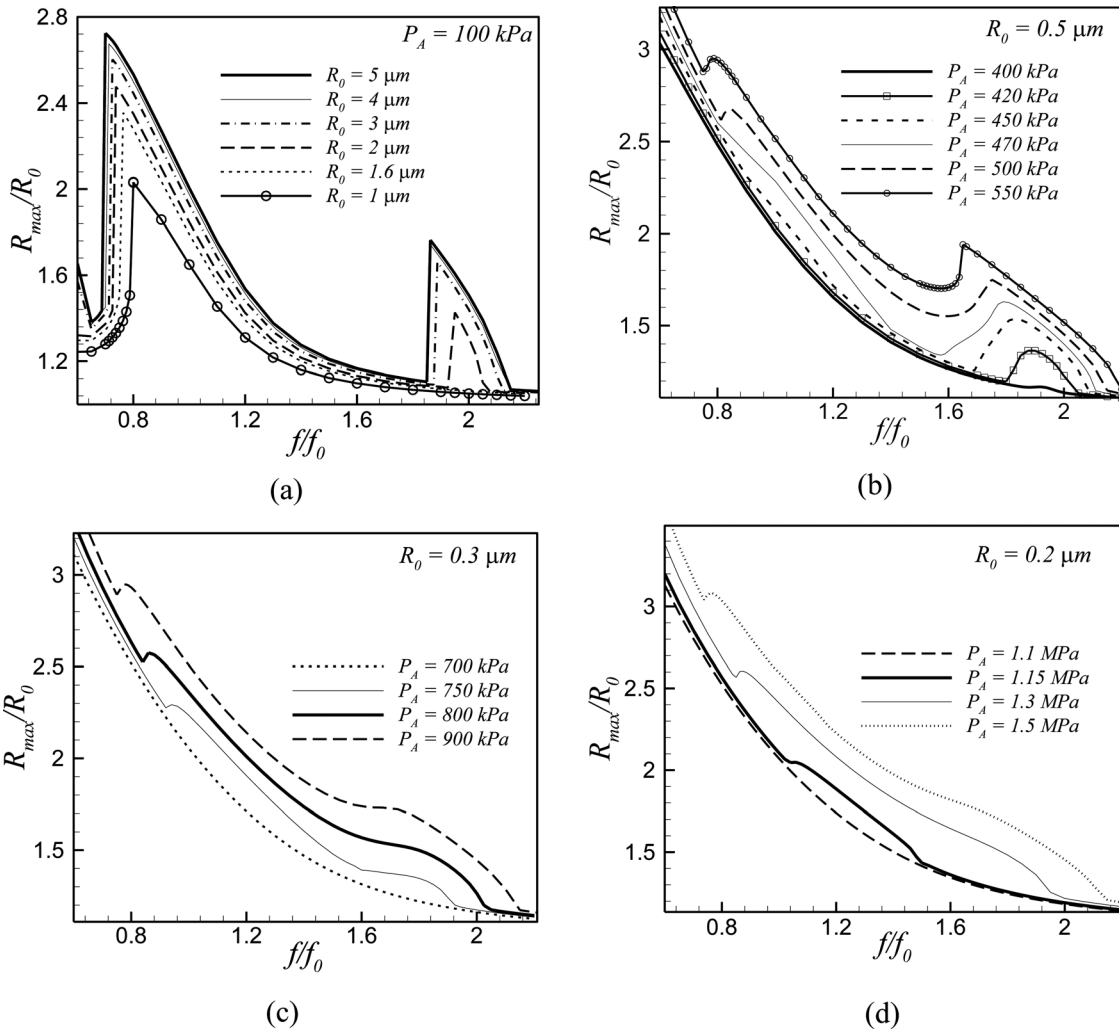


FIG. 2. Frequency response curves for a free bubble (a) at an acoustic pressure = 100 kPa for different initial radii, (b) for $R_0 = 0.5 \mu\text{m}$, (c) $R_0 = 0.3 \mu\text{m}$, and (d) $R_0 = 0.2 \mu\text{m}$ for different acoustic pressures.

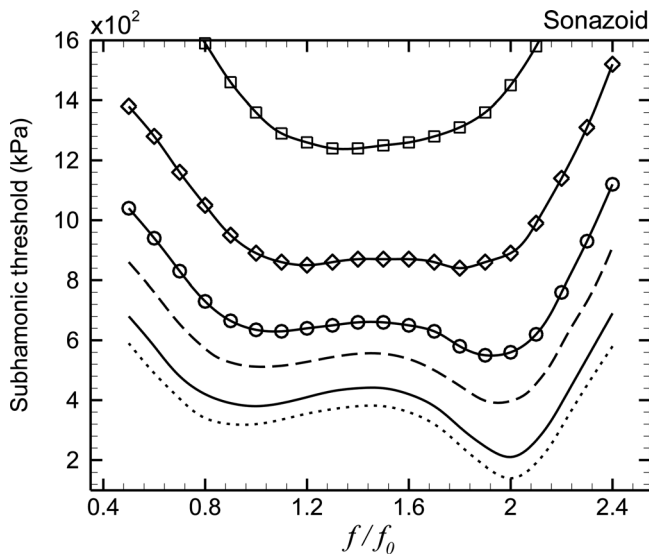


FIG. 3. Variation of the subharmonic threshold of a Sonazoid microbubble [$R_0 = 5 \mu\text{m}$ (.....), $R_0 = 4 \mu\text{m}$ (—), $R_0 = 3 \mu\text{m}$ (---), $R_0 = 2.5 \mu\text{m}$ (—○—), $R_0 = 2 \mu\text{m}$ (—□—), $R_0 = 1.6 \mu\text{m}$ (—◇—)] with normalized excitation frequency as predicted by the Newtonian interfacial rheological model.

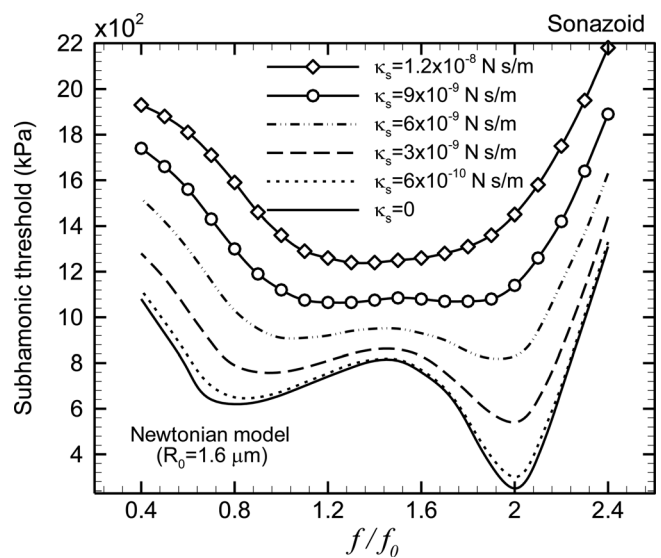


FIG. 4. Variation of the subharmonic threshold of a Sonazoid microbubble ($R_0 = 1.6 \mu\text{m}$) with normalized excitation frequency as predicted by the Newtonian interfacial rheological model for different surface dilatational viscosities (κ_s) of the encapsulation.

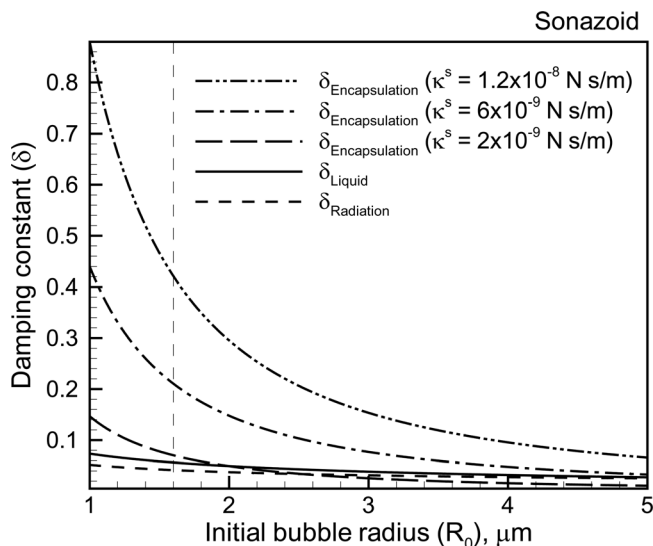


FIG. 5. Variation of damping constants with initial bubble radius for a Sonazoid microbubble as predicted by the Newtonian interfacial rheological model for different surface dilatational viscosity (κ^s) of encapsulation.

at 2–6 MHz (Sarkar *et al.*, 2005). However, a simulated threshold using the entire bubble distribution of Sonazoid matches well with experiment (Paul *et al.*, 2010). As was noted in KS1, the subharmonic response generated at these low excitations is generated by relatively small number of larger bubbles in the bubble distribution having a representative radius of $3 \mu\text{m}$ (the subharmonic response weighted average of Sonazoid). In KS1, we showed the effects of radius variation on the excitation threshold. In the following, we use $R_0 = 3 \mu\text{m}$, and investigate primarily the effects of surface dilatational viscosity.

2. Church–Hoff model

Church–Hoff model is the first rigorous model of the encapsulation where the encapsulation is treated as a finitely thick ($\delta_{\text{sho}} = 3\text{--}20 \text{ nm}$) layer comprising of a viscoelastic material characterized by bulk material properties—shell shear modulus G_s and shear viscosity μ_s (Church, 1995; Hoff *et al.*, 2000). In KS1, we showed that written in an interfacial rheological framework, it has a natural upper limit to its surface tension. Unlike other models, the effective surface dilatational viscosity for this model decreases with the radius. In Fig. 6, we see that similar to the Newtonian model, increasing surface dilatational viscosity leads to a flattening of the threshold curve from having two distinct minima—one at $2f_0$ deeper than the second one at f_0 —to a broader valley around both values.

3. Marmottant model

Marmottant model (Marmottant *et al.*, 2005) is an interfacial rheological model having a dilatational surface viscosity and a dilatational surface elasticity, the latter describing the rate of change of surface tension with changing area fraction. The model is identical to the constant elasticity model proposed shortly earlier (Sarkar *et al.*, 2005), except for the following. Unlike a constant elasticity model, the surface

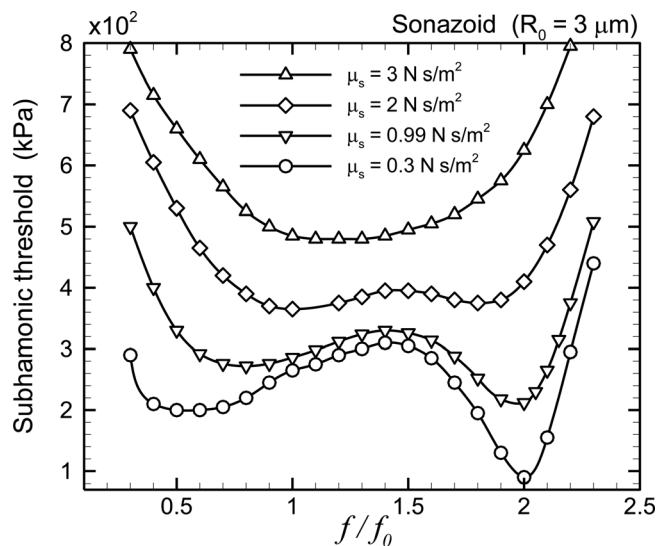


FIG. 6. Variation of the subharmonic threshold of a Sonazoid microbubble ($R_0 = 3 \mu\text{m}$) with normalized excitation frequency as predicted by the Church–Hoff model for different bulk shear viscosity (μ_s) of the encapsulating shell.

tension in the Marmottant model has an upper (ruptured state of the encapsulation with surface tension the same, assuming the value of an air–water interface) and a zero lower (buckled state of the encapsulation) limits. In Fig. 7, we plot the subharmonic threshold predicted by the Marmottant model for varying dilatational viscosity κ^s . As also seen in KS1, the threshold minimum is flatter, and similar to the other models the threshold increases with κ^s . Due to the nonanalytic lower limit of this model, it predicts some distinct behaviors—for lower κ^s values ($\kappa^s = 6 \times 10^{-9} \text{ N s/m}$ and $\kappa^s = 1 \times 10^{-9} \text{ N s/m}$), there is a much lower threshold in the range $1.5 \leq f/f_0 \leq 1.9$. Such an unusually lower threshold has

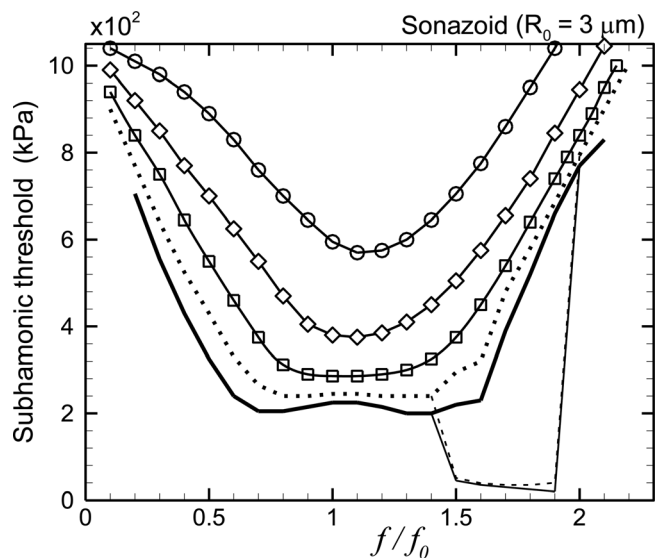


FIG. 7. Variation of the subharmonic threshold of a Sonazoid microbubble ($R_0 = 3 \mu\text{m}$) with normalized excitation frequency as predicted by the Marmottant model [$\kappa^s = 1 \times 10^{-9} \text{ N s/m}$ (—), $\kappa^s = 1 \times 10^{-9} \text{ N s/m}$ (lower threshold) (---), $\kappa^s = 6 \times 10^{-9} \text{ N s/m}$ (lower threshold) (----), $\kappa^s = 6 \times 10^{-9} \text{ N s/m}$ (—□—), $\kappa^s = 1.2 \times 10^{-8} \text{ N s/m}$ (---□---), $\kappa^s = 2 \times 10^{-8} \text{ N s/m}$ (—◇—), and $\kappa^s = 3 \times 10^{-8} \text{ N s/m}$ (—○—)].

been seen experimentally (Frinking *et al.*, 2010). The subharmonic response as a function of excitation for three different frequencies is shown in Fig. 8. It shows for $f/f_0 = 1.7$, a value within the above-mentioned range, appearance of subharmonic at a lower threshold and then its disappearance for intermediate excitation values, and then reappearance at a higher excitation that is more in line with values ($f/f_0 = 1.4, 2$) outside this frequency range. Figure 7 indicates both the lower and the higher thresholds for the smallest two values of κ^s .

4. Exponential elasticity model (EEM)

The EEM model of encapsulation (Paul *et al.*, 2010) assumes the interface to be viscoelastic having a dilatational elasticity and a dilatational viscosity just like the constant elasticity model (Sarkar *et al.*, 2005), but incorporates the effects of strain softening by letting the interfacial elasticity decrease exponentially with increasing surface area. This model, unlike the constant elasticity model and the de Jong model, has an upper limit on the effective interfacial tension which, we noted in KS1, facilitates generation of subharmonic signal near the resonance frequency. In KS1 we showed the effects of variation of the initial radius ($R_0 = 2\text{--}5\ \mu\text{m}$) on frequency-dependent subharmonic threshold. We found for $R_0 \geq 4\ \mu\text{m}$, subharmonic threshold is minimum near twice the resonance frequency, whereas for $R_0 \leq 3\ \mu\text{m}$, subharmonic threshold is minimum near the resonance frequency. Such results can be explained based on the increase in system damping due to the decrease of initial radius (R_0). Here, in Fig. 9, we plot frequency-dependent subharmonic threshold for $R_0 = 3\ \mu\text{m}$ varying κ^s in the range 1×10^{-9} – 3×10^{-8} N s/m. Just like other models, increased encapsulation damping shifts the minimum threshold away from $2f_0$. For $\kappa^s > 1.2 \times 10^{-8}$ N s/m, threshold near twice the resonance increases and thereby the minimum threshold is obtained near the resonance

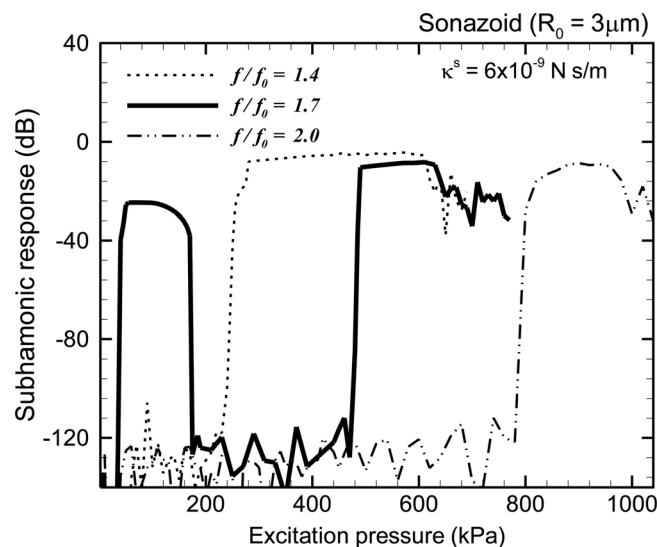


FIG. 8. Subharmonic response as a function of excitation pressure at a low damping ($\kappa^s = 6 \times 10^{-9}$ N s/m) for the Marmottant model. It shows an uncharacteristically low subharmonic threshold at 35 kPa at $f/f_0 = 1.7$. For increasing excitation, the subharmonic later disappears and then reappears at a later value of 480 kPa. For the other two frequency ratios $f/f_0 = 1.4$ and $f/f_0 = 2.0$, there is only one threshold at 240 and 780 kPa, respectively.

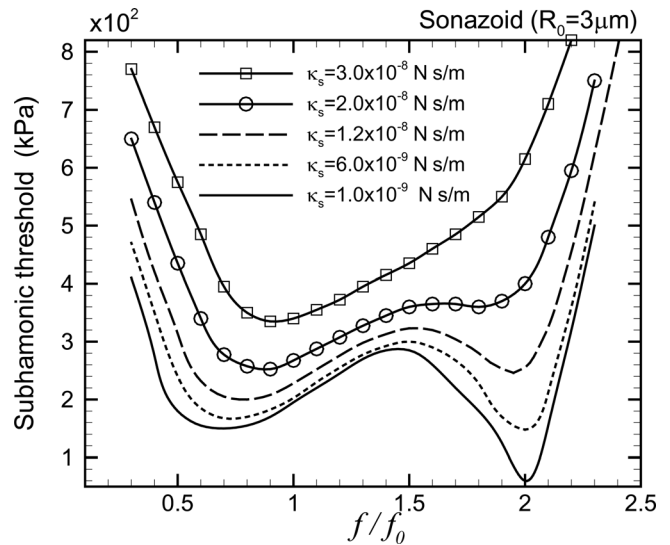


FIG. 9. Variation of the subharmonic threshold of a Sonazoid microbubble $R_0 = 3.0\ \mu\text{m}$ with normalized excitation frequency as predicted by viscoelastic exponential elasticity model (EEM) for different surface dilatational viscosity (κ^s) of encapsulation.

frequency. On the other hand, for $\kappa^s < 1.2 \times 10^{-8}$ N s/m, the minimum threshold near twice the resonance frequency gets sharpened.

IV. SUMMARY AND CONCLUSIONS

In a recent investigation (KS1), we found that contrary to the classical result, the minimum excitation threshold for subharmonic generation from contrast microbubbles, according to a number of different models of encapsulation, does not necessarily occur at twice the resonance frequency, but shifts to lower frequencies. Subsequently, an experimental investigation also found subharmonic threshold at resonance frequency lower than at twice the resonance (Faez *et al.*, 2012). In KS1, we expressed all models in a common interfacial rheological form containing a radius-dependent effective surface tension $\gamma(R)$ and an effective dilatational viscosity $\kappa^s(R)$. For most encapsulation models, the dilatational surface viscosity is constant. The study concentrated on the effects of the form of effective surface tension $\gamma(R)$ on the subharmonic threshold. Here, we further investigate this phenomenon seeking an explanation of the deviation from the classical result in the damping of the encapsulation. We note that the damping contribution due to encapsulation is an order of magnitude larger than the other damping terms—due to liquid viscosity and re-radiation.

A damped linear oscillator has a natural frequency lower than that of an undamped oscillator. We first seek an explanation of the shift of the minimum threshold to lower frequencies in the decreased linear natural frequency due to damping. However, we show that the frequency for maximum scattered pressure (as opposed to maximum displacement) actually increases with increasing damping. The simple shift of natural frequency of the linearized system due to damping, therefore, cannot explain the result in KS1. Instead, we examine the complete nonlinear bubble dynamics according to a number of different models—free bubble, Newtonian, Church–Hoff,

Marmottant, and exponential elasticity—varying the radius as well as the surface dilatational viscosity of the encapsulation. These models were shown in KS1 to predict subharmonic threshold values comparable to experimental observations.

The damping of the bubble dynamics increases sharply with decreasing bubble radius. We show that the subharmonic threshold increases with increasing damping—the threshold near twice the resonance frequency increases more than the one near the resonance frequency. Therefore, even for a free bubble, the minimum threshold shifts to the resonance frequency from twice the resonance for smaller sub-micron radii. For contrast microbubbles, the total damping is dominated by that arising from the encapsulation, modeled by the dilatational viscosity. One sees results similar to free bubbles for Newtonian, Church–Hoff, and exponential elasticity models—the minimum threshold at twice the resonance shifts to resonance with increasing damping. The Marmottant model shows a flatter response with a valley of threshold minima in the range of frequencies from resonance to twice its value; its value increases with increasing dilatational viscosity. Due to the nondifferentiable character of the surface tension at its lower limit (imposed to ensure non-negative surface tension), it has some distinctive features at low values of damping. It has an extremely low threshold of subharmonic generation, as also noted before (Frinking *et al.*, 2010), and then the disappearance of subharmonic at an intermediate pressure, and then the reappearance at a higher pressure. Note that a non-negative surface tension cannot explain the stability of contrast microbubbles—bubbles with non-negative surface tension are only neutrally stable against dissolution (Katiyar and Sarkar, 2010). After all, the encapsulation stabilizes a contrast microbubble (Katiyar *et al.*, 2009; Sarkar *et al.*, 2009). Further, a negative surface stress, i.e., a net compressive stress is what causes the encapsulation to buckle.

We conclude that encapsulated microbubbles due to their small size and the encapsulation contain significant damping. The deviation from the classical result of minimum threshold at twice the resonance frequency occurs for them because the classical results are obtained using perturbation analysis that assumes small damping. Increased damping reduces response at twice the resonance frequency more than at resonance frequency shifting the minimum threshold excitation for subharmonic generation toward the resonance frequency. The subharmonic signal is generated by energy transfer between frequencies intrinsic to a nonlinear system. The classical perturbative result arises from the ease of amplification of the natural frequency component, while being excited at twice the resonance frequency. The higher damping at twice the resonance compared to at resonance competes with this effect resulting ultimately in the shift of the minimum. Note that the numerical study presented here is not limited to any particular model of the encapsulation. It does not account for nonspherical oscillation—recently high speed optical observation has shown parametrically driven shape oscillation in contrast microbubbles at subharmonic frequencies (Dollet *et al.*, 2008). However, we contend that although the bubble wall indeed undergoes strong shape oscillations, they give rise to a dipole pressure field in contrast to the monopole due

to the radial pulsation, and therefore have very little effect on the scattered far field response recorded by a transducer situated away from the bubble. Also note that although the overall subharmonic threshold for a specific contrast agent is determined by the entire bubble size distribution, the underlying physics can only be understood by single bubble behavior focused here. After all, the classical theoretical result is based on single bubble dynamics. Finally, the recent experimental observation (Faez *et al.*, 2012) of lower subharmonic generation threshold at resonance than at twice the resonance clearly demonstrates the phenomenon explained here.

ACKNOWLEDGMENTS

The authors acknowledge helpful discussions with Professor Flemming Forsberg. This work is partially supported by NSF Grant Nos. CBET-0651912, CBET-1033256, and DMR-1005283 and NIH Grant No. P20RR016472.

- Adam, D., Sapunar, M., and Burla, E. (2005). “On the relationship between encapsulated ultrasound contrast agent and pressure,” *Ultrasound Med. Biol.* **31**, 673–686.
- Andersen, K. S., and Jensen, J. A. (2010). “Impact of acoustic pressure on ambient pressure estimation using ultrasound contrast agent,” *Ultrasonics* **50**, 294–299.
- Chatterjee, D., Jain, P., and Sarkar, K. (2005a). “Ultrasound-mediated destruction of contrast microbubbles used for medical imaging and drug delivery,” *Phys. Fluids* **17**, 100603.
- Chatterjee, D., and Sarkar, K. (2003). “A Newtonian rheological model for the interface of microbubble contrast agents,” *Ultrasound Med. Biol.* **29**, 1749–1757.
- Chatterjee, D., Sarkar, K., Jain, P., and Schreppler, N. E. (2005b). “On the suitability of broadband attenuation measurement for characterizing contrast microbubbles,” *Ultrasound Med. Biol.* **31**, 781–786.
- Church C. C. (1995). “The effects of an elastic solid-surface layer on the radial pulsations of gas-bubbles,” *J. Acoust. Soc. Am.* **97**, 1510–1521.
- Dave, J. K., Halldorsdottir, V. G., Eisenbrey, J. R., Liu, J. B., McDonald, M. E., Dickie, K., Leung, C., and Forsberg, F. (2011). “Noninvasive estimation of dynamic pressures *in vitro* and *in vivo* using the subharmonic response from microbubbles,” *IEEE Trans. Ultrason. Ferroelectr. Freq. Contr.* **58**, 2056–2066.
- de Jong, N. (1996). “Improvements in ultrasound contrast agents,” *IEEE Eng. Med. Biol. Mag.* **15**, 72–82.
- de Jong, N., Cornet, R., and Lancee, C. T. (1994). “Higher harmonics of vibrating gas-filled microspheres. 1. Simulations,” *Ultrasonics* **32**, 447–453.
- Dollet, B., van der Meer, S. M., Garbin, V., de Jong, N., Lohse, D., and Versluis, M. (2008). “Nonspherical oscillations of ultrasound contrast agent-microbubbles,” *Ultrasound Med. Biol.* **34**, 1465–1473.
- Eller, A., and Flynn, H. G. (1968). “Generation of subharmonics of order 1-half by bubbles in a sound field,” *J. Acoust. Soc. Am.* **44**, 368–369.
- Faez, T., Emmer, M., Docter, M., Sijl, J., Versluis, M., and de Jong, N. (2011). “Characterizing the subharmonic response of phospholipid-coated microbubbles for carotid imaging,” *Ultrasound Med. Biol.* **37**, 958–970.
- Faez, T., Skachkov, I., Versluis, M., Kooiman, K., and de Jong, N. (2012). “*In vivo* characterization of ultrasound contrast agents: microbubble spectroscopy in a chicken embryo,” *Ultrasound Med. Biol.* **38**, 1608–1617.
- Ferrara, K., Pollard, R., and Borden, M. (2007). “Ultrasound microbubble contrast agents: Fundamentals and application to gene and drug delivery,” *Annu. Rev. Biomed. Eng.* **9**, 415–447.
- Forsberg, F., Liu, J. B., Shi, W. T., Furuse, J., Shimizu, M., and Goldberg, B. B. (2005). “*In vivo* pressure estimation using subharmonic contrast microbubble signals: Proof of concept,” *IEEE Trans. Ultrason. Ferroelectr. Freq. Contr.* **52**, 581–583.
- Forsberg, F., Shi, W. T., and Goldberg, B. B. (2000). “Subharmonic imaging of contrast agents,” *Ultrasonics* **38**, 93–98.
- Frinking, P. J. A., Gaud, E., and Arditi, M. (2010). “Subharmonic scattering of phospholipid-shell microbubbles at low acoustic pressure amplitudes,” *IEEE Trans. Ultrason. Ferroelectr. Freq. Contr.* **57**, 1762–1771.

- Goldberg, B. B., Raichlen, J. S., and Forsberg, F. (2001). *Ultrasound Contrast Agents: Basic Principles and Clinical Applications*, 2nd ed. (Martin Dunitz, London).
- Hoff, L., Sontum, P. C., and Hovem, J. M. (2000). "Oscillations of polymeric microbubbles: Effect of the encapsulating shell," *J. Acoust. Soc. Am.* **107**, 2272–2280.
- Katiyar, A., and Sarkar, K. (2010). "Stability analysis of an encapsulated microbubble against gas diffusion," *J. Coll. Interf. Sci.* **343**, 42–47.
- Katiyar, A., and Sarkar, K. (2011). "Excitation threshold for subharmonic generation from contrast microbubbles," *J. Acoust. Soc. Am.* **130**, 3137–3147.
- Katiyar, A., Sarkar, K., and Forsberg, F. (2011). "Modeling subharmonic response from contrast microbubbles as a function of ambient static pressure," *J. Acoust. Soc. Am.* **129**, 2325–2335.
- Katiyar, A., Sarkar, K., and Jain, P. (2009). "Effects of encapsulation elasticity on the stability of an encapsulated microbubble," *J. Coll. Interface Sci.* **336**, 519–525.
- Kimmel, E., Krasovitski, B., Hoogi, A., Razansky, D., and Adam, D. (2007). "Subharmonic response of encapsulated microbubbles: Conditions for existence and amplification," *Ultrasound Med. Biol.* **33**, 1767–1776.
- Lauterborn, W. (1976). "Numerical investigation of nonlinear oscillations of gas-bubbles in liquids," *J. Acoust. Soc. Am.* **59**, 283–293.
- Leodore, L., Forsberg, F., and Shi, W. T. (2007). "Subharmonic contrast microbubble signals for Noninvasive pressure estimation: An *in vitro* study," *Circulation* **116**, 646–646.
- Marmottant, P., van der Meer, S., Emmer, M., Versluis, M., de Jong, N., Hilgenfeldt, S., and Lohse, D. (2005). "A model for large amplitude oscillations of coated bubbles accounting for buckling and rupture," *J. Acoust. Soc. Am.* **118**, 3499–3505.
- Paul, S., Katiyar, A., Sarkar, K., Chatterjee, D., Shi, W. T., and Forsberg, F. (2010). "Material characterization of the encapsulation of an ultrasound contrast microbubble and its subharmonic response: Strain-softening interfacial elasticity model," *J. Acoust. Soc. Am.* **127**, 3846–3857.
- Prosperetti, A. (1976). "Subharmonics and ultraharmonics in forced-oscillations of weakly nonlinear-systems," *Am. J. Phys.* **44**, 548–554.
- Prosperetti, A. (1977). "Application of subharmonic threshold to measurement of damping of oscillating gas-bubbles," *J. Acoust. Soc. Am.* **61**, 11–16.
- Sarkar, K., Katiyar, A., and Jain, P. (2009). "Growth and dissolution of an encapsulated contrast microbubble," *Ultrasound Med. Biol.* **35**, 1385–1396.
- Sarkar, K., Shi, W. T., Chatterjee, D., and Forsberg, F. (2005). "Characterization of ultrasound contrast microbubbles using *in vitro* experiments and viscous and viscoelastic interface models for encapsulation," *J. Acoust. Soc. Am.* **118**, 539–550.
- Shankar, P. M., Krishna, P. D., and Newhouse V. L. (1998). "Advantages of subharmonic over second harmonic backscatter for contrast-to-tissue echo enhancement," *Ultrasound Med. Biol.* **24**, 395–399.
- Shankar, P. M., Krishna, P. D., and Newhouse, V. L. (1999). "Subharmonic backscattering from ultrasound contrast agents," *J. Acoust. Soc. Am.* **106**, 2104–2110.
- Shi, W. T., Forsberg, F., Raichlen, J. S., Needleman, L., and Goldberg, B. B. (1999). "Pressure dependence of subharmonic signals from contrast microbubbles," *Ultrasound Med. Biol.* **25**, 275–283.
- Sijl, J., Dollet, B., Overvelde, M., Garbin, V., Rozendal, T., de Jong, N., Lohse, D., and Versluis, M. (2010). "Subharmonic behavior of phospholipid-coated ultrasound contrast agent microbubbles," *J. Acoust. Soc. Am.* **128**, 3239–3252.
- Tang, M. X., Mulvana, H., Gauthier, T., Lim, A. K. P., Cosgrove, D. O., Eckersley, R. J., and Stride, E. (2011). "Quantitative contrast-enhanced ultrasound imaging: A review of sources of variability," *Interface Focus* **1**, 520–539.
- van der Meer, S. M., Dollet, B., Voormolen, M. M., Chin, C. T., Bouakaz, A., de Jong, N., Versluis, M., and Lohse, D. (2007). "Microbubble spectroscopy of ultrasound contrast agents," *J. Acoust. Soc. Am.* **121**, 648–656.